Multi-omics uncovers molecular targets for reef restoration from heat evolved strains of a host-generalist species of dinoflagellate (Cladocopium, Symbiodiniaceae)

Katie E. Hillyer

Katie.hillyer@detsi.qld.gov.au

Commonwealth Scientific and Industrial Research Organisation (CSIRO)

Patrick Buerger

Macquarie University

Sarah-Jane Tsang Min Ching

University of Melbourne

Jian-Wei Liu

CSIRO Environment

David J. Beale

Commonwealth Scientific and Industrial Research Organisation (CSIRO)

Research Article

Keywords: Multi-omics, coral, holobiont, symbiosis, bleaching

Posted Date: May 11th, 2026

DOI: https://doi.org/10.21203/rs.3.rs-9479808/v1

Additional Declarations: No competing interests reported.

Abstract

Climate change has increased coral bleaching, transforming coral reefs. While reef restoration techniques through heat-evolved symbionts have shown promise, the mechanisms for enhanced symbiosis and targets for improvement remain unclear.

Using integrated multi-omics, we explored differences in metabolite, lipid, and protein of the model anemone host (*Exaiptasia diaphana*) in symbiosis with multiple strains of the host generalist, *Cladocopium proliferum* (Symbiodiniaceae) under ambient conditions. Analysed strain partnerships comprised two strains that were laboratory heat evolved, one which has been shown to improve thermal tolerance *in hospite* (SS8), one that did not (SS5), and the wildtype (WT10).

Multi-block analysis revealed characteristic differences in 30 proteins, 20 lipids, and 6 metabolites. SS8 hosts were most differentiated from WT10, and to a lesser extent SS5. Key analytes characterising SS8 partnerships comprised those associated with the metabolism of the antioxidant glutathione, glucose, arachidonic acid, tryptophan, diacylglycerol lipids, nitrogen and purine.

At a pathway level, differences between partnerships were primarily observed in expression of metabolites and proteins associated with metabolism, in addition to environmental information processing, cellular process, and genetic information processing. SS8 partnerships were once again most differentiated in the metabolism of carbon, glutathione, amino acid, and nitrogen; and pathways related to signalling, including phosphatidylinositol, heterotrophy, recognition, phagocytosis, transmembrane transport, and lysosomal activity.

These results offer insight into complex functional implications of laboratory evolved symbionts in a model system. They also highlight targets to facilitate rapid and successful symbiont establishment, maintenance, and mechanisms for responding to environmental change in the holobiont.

Introduction

Coral bleaching due to climate change is transforming coral reefs (Hughes et al. 2018; Hughes et al. 2019). With annual major bleaching events projected to be the new normal, interventions to '*engineer*' enhanced coral phenotypes and assist coral survival are becoming more important for coral conservation (Anthony et al. 2017; van Oppen and Blackall 2019). Bleaching tolerance can be enhanced via natural adaptation or acclimation (Palumbi et al. 2014), and interventions, such as human-assisted evolution (van Oppen et al. 2015; Cleves 2022), and potentially other biotechnological solutions (van Oppen et al. 2015; Anthony et al. 2017; Cleves 2022). Experimental evolution of Symbiodiniaceae strains to enhance their own and the corals thermal tolerance has been one recent focus for reef restoration (Nitschke et al. 2024).

Cladocopium proliferum (Symbiodiniaceae) is a host-generalist species of dinoflagellate that is mutualistic with Indo-Pacific reef corals (Butler et al. 2023). It was identified as a potential target for

laboratory heat-evolution, isolated from the inshore Great Barrier Reef (Australia) from the common scleractinian coral *Acropora kenti* and cultured under elevated temperature for over 80 generations (2.5 years), producing 10 heat-evolved strains (Chakravarti et al. 2017). After roughly 120 generations (4 years), all 10 strains showed enhanced thermal tolerance *in vitro*, maintaining growth and secreting lower concentrations of reactive oxygen species (ROS), however only three strains were observed to enhance thermal bleaching tolerance in *A. kenti* larvae (Buerger et al. 2020). Subsequent studies with a sub-set of the same strains, found no growth trade-offs at ambient temperature in *A. kenti* juveniles (Quigley et al. 2023), and *Galaxea fascicularis (*Chan et al. 2023). However, differences were observed *in hospite* between wild-type and heat-evolved strains in algal pigments (Chan et al. 2023), and rates of photosynthesis and carbon fixation (Buerger et al. 2020). Further, when in symbiosis with the coral model, *E. diaphana*, differences in nitrogen metabolism were also observed between strains (Tsang Min Ching et al. 2022). Gaps however remain in understanding of opportunities optimising these heat-evolved partners, relevant to holobiont performance both under ambient conditions, and those of thermal stress.

For coral holobionts to function there must be a complex interplay between the cnidarian host, photosymbionts and other associated microbes; this communication network operates at sub-cellular to multiple cellular scales, from RNA to complex proteins, metabolites and lipids (Rosset et al. 2021). The communication system likely enables rapid detection, and dynamic responses to changes in holobiont function, e.g., associated differences in mobile product translocation (Hillyer et al. 2018). Similarly, these diverse mechanisms also likely enable detection and cellular management of sub-optimal partnerships and their proliferation, for instance, via the limitation of nutrients that are translocated between the symbiont partners (Cui et al. 2019; Xiang et al. 2020). Multi-omics approaches are already being used to develop intervention strategies, via improved understanding of targets for trait improvement, in a range of agricultural and clinical settings (Iqbal et al. 2021), and host microbiome interactions (Yan et al. 2022). Interventions that target enhanced coral resilience will require more detailed and holistic insight of symbiosis establishment, regulation, and functioning.

The symbiotic anemone *E. diaphana* is widely applied as a model for cnidarian-dinoflagellate symbiosis function (Weis et al. 2008), increasingly using highly detailed and sensitive omics based approaches including proteomics (Oakley et al. 2016), lipidomics (Garrett et al. 2011; Garrett et al. 2013), and metabolomics (Burriesci et al. 2012; Hillyer et al. 2017). These omics based tools have also been applied to investigate functional change in the cnidarian-dinoflagellate symbiosis associated with experimentally introduced (heterologous) (Matthews et al. 2018; Sproles et al. 2019), and heat-evolved photosymbionts (Tsang Min Ching et al. 2022). However, at a system level to better understand the interplay between holobiont members, multi-omics approaches offer additional insight into the cellular mechanisms that influence a holobiont's thermal tolerance, one such mechanism is the production of lower levels of ROS *in hospite* (Cziesielski et al. 2018; Maruyama et al. 2021; Liang et al. 2022). Hence, multi-omics approaches enable rapid targeting and validation of possible intervention strategies, holistically determining functional implications to the holobiont with greater confidence.

Using a multi-omics approach in the model anemone, *E. diaphana*, we further investigate the restoration potential and functional implications of experimentally introduced, heat-evolved *C. proliferum* symbionts, under ambient conditions. Specifically, a heat-evolved strain previously shown to enhance thermal tolerance (SS8), a heat-evolved strain that did not (SS5) (Buerger et al. 2020), and the wild-type (WT10). After the anemones were in symbiosis with the respective strains for 9 weeks, we applied a discovery-based (untargeted) multi-omics approach, coupling proteomics, lipidomics, and metabolomics, in order to further examine differences in potential molecular targets.

Results

At the time of multi-omics sampling, 9 weeks post inoculation, sampled anemone weights were similar between partnerships (Fig. 1a). However, symbiont densities differed between strains (Kruskal Wallis: $H_{2,12} = 8$, $P = 0.0048$; Fig. 1b), with the lowest densities observed in the SS8 partnership (cells mg^{-1} host protein ± SEM: WT10: 96,196 ± 16,343; SS5: 30,644 ± 5,435; SS8: 20,240 ± 7,271).

Multi-omics analysis

Multi-block PLS-DA (DIABLO) analysis of the entire dataset revealed differences in host protein, lipid, and metabolite fractions associated with the respective photosymbiont strain (Fig. 2). The greatest dissimilarity was observed between *E. diaphana* in symbiosis with WT10 and SS8 (dimension 1), with separation of the SS5 hosts along the second dimension (dimension 2). On dimension 1, identified variables best explaining dissimilarity between WT10 vs SS8 hosts, comprised 30 proteins, 20 lipids, and 6 metabolites (Table S1).

Dimension 1

Of the 30 identified proteins, 6 were associated with glutathione metabolism and were upregulated in SS8 hosts. The most influential glutathione associated proteins to dissimilarity (DIABLO variable value: 0.30) were transferases including, glutathione S-transferase, and glutathione S-transferase Mu 5-like (Fig. 3a).

Other influential upregulated proteins explaining dissimilarity identified in the analysis (DIABLO variable value: 0.31 to 0.25), comprised those associated with the metabolism of glucose (phosphoglucomutase-1), polyunsaturated fatty acid (arachidonic acid; prostaglandin reductase 2), and the amino acid, tryptophan (3-hydroxyanthranilate 3,4-dioxygenase, kynurenine-oxoglutarate transaminase 3) (Fig. 3b).

Whereas only explanatory decline in protein expression in SS8 host's relative to WT10 (DIABLO variable value: -0.20), was associated with ammonia recycling and nitrogen metabolism, glutamine synthetase (Fig. 3c).

The most influential lipids (DIABLO variable value: -0.49 to -0.16) showed declines in abundance in SS8 hosts relative to WT10, these were primarily diacylglycerols, DG.17.1.9Z..18.0.0.0, DG.17.2.9Z.12Z..18.3,

and DG.19.1.9Z..20.5.5Z (Fig. 4a).

Similarly, in the metabolite dataset, declines in abundance best characterised differences between SS8 hosts relative to WT10 (DAIBLO variable value: -0.65 to -0.38), specifically those associated with electron transfer (beta-nicotinamide adenine dinucleotide), and purine biosynthesis (pterine, guanosine) (Fig. 4b).

Dimension 2

Explaining dissimilarity of SS5 host types in dimension 2, the majority of identified variables comprised 50 lipids across a range of classes, with 7 metabolites, and 5 proteins (Table S2). Of these lipids, 44 were decreased in SS5 hosts, the most influential being a glycerophospholipid, PA.O.16.0.20.5.5Z.8Z (DIABLO variable value: 0.36). All of the DIABLO identified metabolites were also decreased in SS5 hosts, the most influential being the phytochemical, cynaroside A (DIABLO variable value: 0.51).

Whereas all identified proteins from the DIABLO analysis were upregulated in SS5 hosts relative to WT10 (DIABLO variable value: -0.65 to -0.12, Fig. 5). The most influential were associated with oxidative phosphorylation (NADH dehydrogenase [ubiquinone]), signal transduction (low-density lipoprotein receptor-related protein 4), the aminopeptidase, glutamyl aminopeptidase, in addition to those associated with iron storage (soma ferritin), and carbon concentration (carbonic anhydrase 2).

KEGG pathways

Significant metabolite and protein fold changes between partnerships (Table 1) were mapped to KEGG pathways for *E. diaphana* to explore wider pathway implications. Consistently enriched gene ontology terms revealed differences in pathway classifications between partnerships across metabolism (72.62–74.42%), environmental information processing (9.30–10.72%), and cellular process and genetic information processing (5.81–9.52%).

Table 1
Total number of significant fold changes in each analyte class between strains

Strain comparison		**Metabolite**		**Lipid**		**Protein**	
		-	**+**	**-**	**+**	**-**	**+**
WT10	SS5	54	21	22	3	151	106
	SS8	41	25	45	2	191	126
SS5	SS8	24	51	10	7	126	77

Fold change differences in multiple analytes were observed to seven major pathways (Table 2) associated with the metabolism of carbon (Fig S1), glutathione (Fig S2), and amino acids, the biosynthesis of amino acids, and the creatine pathway (Fig S3), in addition to pathways associated with heterotrophy, cell signalling, recognition, phagocytosis, transmembrane transport, and lysosomal activity.

Of these key pathways, significantly altered analytes that were also identified in the DIABLO analysis and upregulated in all comparisons were proteins associated with the metabolism of valine (3-hydroxyisobutyryl-CoA, log2FC 1.52–3.92), and glutathione (glutathione S-transferase, log2FC 1.03–3.43). In both instances, the largest upregulation of these proteins was observed between SS8 relative to WT10. Additionally, for SS8 comparisons only, this was coupled to a downregulation of glutamine synthetase (log2FC -1.49 to -2.10), a protein critical to nitrogen metabolism and the synthesis of glutamine, from glutamate and ammonia.

Outside of the DIABLO identified analytes consistent change, typically to the greatest extent SS8 relative to WT10, was also observed to carbon associated metabolism (upregulated: galactokinase, homocitrate; downregulated: PEP), glutathione metabolism (downregulated: cytochrome c oxidase), and signalling (downregulated: 5-methoxytryptamine, adenylate cyclase) (Table 2).

In addition to the lipids identified by the DIABLO analysis, widespread fold changes were also observed to proteins associated with transmembrane transport and lysosomal activity. The largest fold change in both select strain hosts relative to WT10 was to the active membrane transporter, major facilitator superfamily (MFS) profile domain-containing protein (an organic cation transporter-like protein; log2FC -6.06). Whereas one glycosidase (lysosomal alpha-glucosidase), and one dehydrogenase (epidermal retinol dehydrogenase 2) were upregulated in the heat evolved partnerships.

Discussion

Via a discovery-led multi-omics approach in the anemone model *E. diaphana*, we investigated the restoration potential, functional implications, and targets for intervention associated with the introduction of heat-evolved *C. proliferum* symbiont strains, relative to WT10 under ambient conditions. Specifically, a heat-evolved strain previously shown to enhance thermal tolerance (SS8), a heat-evolved strain that did not (SS5) (Buerger et al. 2020), and the wild-type (WT10). After the anemones were in symbiosis with the respective strains for 9 weeks, host fractions were analysed via an untargeted approach coupling proteomics, lipidomics, and metabolomics. Sampled anemone weights were similar between partnerships; however, symbiont densities differed between strains, WT10 > SS5>SS8.

Multi-block (DIABLO) analysis revealed the greatest dissimilarity was between *E. diaphana* in symbiosis with WT10 and SS8 and identified variables best explaining this dissimilarity which comprised 30 proteins, 20 lipids, and 6 metabolites. SS5 hosts were differentiated to a lesser extent, primarily by 50 lipids, 7 metabolites, and 5 proteins. Further exploring differences in the relative abundance of individual analytes, significant fold changes were explored at a pathway level. Change was observed to seven major pathways associated with the metabolism of carbon, glutathione, and amino acids, the biosynthesis of amino acids, and the creatine pathway, in addition to pathways associated with heterotrophy, cell signalling, recognition, phagocytosis, transmembrane transport, and lysosomal activity.

Carbon metabolism

We observed characteristic differences in carbon metabolism in heat-evolved SS8 partnerships relative to WT10 and SS5, in addition to proteins associated with their transmembrane transport (see below), indicative of differences in symbiont derived products of photosynthesis (carbohydrate and/or lipid), the generation of carbon-based ATP and reducing power (NADPH/NADH), and downstream biosynthesis pathways.

The glycolysis associated enzyme, phosphoglucomutase-1, which catalyses the reversible interconversion of glucose-1-phosphate and glucose-6-phosphate (phosphoglucomutase-1), best explained SS8 host dissimilarity of all available analysed proteins (DIABLO analysis), in addition to other glycolysis, and glyoxylate associated proteins. At a pathway level in SS8 hosts, upregulation of proteins associated with glycolysis, sugar metabolism, carbohydrate degradation, galactose, and glyoxylate metabolism was observed, coupled to declines in the relative abundance of glycolytic intermediates (D-glucosamine 6-phosphate, PEP, glyceric acid), and diacylglycerol lipids. Change in SS5 partnerships was less widespread, however upregulation of a protein associated with carbon concentration (carbonic anhydrase 2) and oxidative phosphorylation (NADH dehydrogenase) characterised SS5 dissimilarity (DIABLO analysis).

The upregulation of host glycolysis and catabolic pathways for alternative energy generation is indicative of differences in mobile product provision and/or respiratory costs associated with heat-evolved SS8, relative to WT10 and SS5. A decline in the quantity and/or quality of mobile product translocation from photosynthesis would necessitate host energy generation from alternative sources, such as the breakdown of lipid and carbohydrate energy stores, and/or increased heterotrophy (as discussed below), as observed during thermal stress and low symbiont levels during bleaching (Hillyer et al. 2016). Importantly in the context of thermal resistance, an increase in host energy generation via anaerobic glycolysis, may also serve to limit production of respiratory associated ROS, which would otherwise be generated during oxidative phosphorylation (Chan et al. 2025).

At the time of sampling (9 weeks post inoculation), anemone weights were similar between partnerships, however symbiont densities differed, being highest in WT10, and lowest in the SS8 partnership, with SS5 intermediate. This likely affected the quantity of symbiont derived products of photosynthesis overall. In addition, both heat-evolved symbiont strains when *in hospite* in coral larvae demonstrated downregulated photosynthesis genes (Buerger et al. 2020). However, targeted analysis of central carbon metabolites in multiple heat-evolved *E. diaphana* partnerships (enhanced bleaching tolerance SS1, SS7 and SS8, and non-enhanced, SS3, SS5 and SS9) (Tsang Min Ching et al. 2022), detected few differences in the relative abundance of analytes in symbiont and host partners relative to WT10. As such, no trade-off in symbiont mobile product provision was concluded in *E. diaphana* relative to WT10 (Tsang Min Ching et al. 2022). However, this use of multiple heat-evolved partnerships may have masked larger differences present in the current study, as apparent in the differing cell densities of SS8 v SS5 at the time of sampling. Further, in the current study, the ability to detect smaller differences would be expected given the high sensitivity of the platform applied (Liquid Chromatography Quadrupole Time-of-Flight Mass Spectrometry) and multi-omics approach herein.

The upregulation carbonic anhydrase 2, in SS5 partnerships is also notable. This protein is associated with carbon concentration mechanisms upregulated in both homologous and heterologous symbiont associations (Sproles et al. 2019), upregulation may therefore serve to stimulate additional symbiont photosynthesis in the SS5 partnership, coupled with upregulation of oxidative phosphorylation (NADH dehydrogenase) for enhanced generation of cellular ATP relative to WT10, as reflected in the less extensive changes in SS5 partnerships relative to SS8.

Differences in the relative abundance of diacylglycerol (glycerolipids) lipids also characterised the two heat evolved partnerships, with negative fold changes relative to WT10, primarily the diacylglycerols, DG(17:1(9Z)/18:0/0:0), DG(17:2(9Z,12Z)/18:3(9Z,12Z,15Z)/0:0), and DG(19:1(9Z)/20:5(5Z,8Z,11Z,14Z,17Z)/0:0). Diacylglycerol lipids have a diverse range of functions and associated pathways, including as components of cellular membranes, as building blocks for glycero(phospho)lipids, and as lipid second messengers (Eichmann and Lass 2015). Lipids comprise a critical component of symbiont derived products of photosynthesis, and host lipid profiles are characteristic of symbiont community composition (Garrett et al. 2011; Garrett et al. 2013).

Characteristic differences in these lipids are therefore likely indicative of change associated with the availability of symbiont derived products of photosynthesis (both carbohydrate and lipid), downstream host biosynthesis, and signalling pathways (as discussed below).

Glutathione metabolism and oxidative phosphorylation

Increased expression of proteins related to the metabolism of the antioxidant glutathione (GSH) characterised dissimilarity of SS8 hosts, relative to WT10 and SS5 (DIABLO analysis). Specifically, the transferases, glutathione S-transferase, and glutathione S-transferase Mu 5-like. Coupled to this we observed a down regulation of mitochondrial proteins associated with oxidative phosphorylation and the generation of cellular ATP in SS8 hosts, including V-type proton ATPase, ATP synthase subunit O, cytochrome c oxidase, and cytochrome b-c1 complex.

In previous studies, both SS5 and SS8, produced lower levels of ROS during acute heat exposure in culture relative to wild type strains; however, SS8 was considered as heat tolerant in coral larvae, with stable cell numbers and photosystem health, whereas SS5 was considered heat sensitive (Buerger et al. 2020). Differences were attributed to rates of symbiont photosynthesis, and with SS8, the increased expression of host heat stress genes, including glutathione S-transferase, potential front-loading prior to thermal stress (Buerger et al. 2020). Under conditions of thermal stress *E. diaphana* hosting SS8 exhibited the highest thermotolerance, relative to five other heat-evolved strains (SS1, SS3, SS5, SS7, SS9), with WT10 the second most thermally tolerant group, and heat-evolved SS5 strain amongst the most thermosensitive (Chan et al. 2025). Accordingly, metabolites associated with the antioxidant, glutathione, and polyol antioxidants showed the greatest fold changes in SS8 hosts, with WT10 hosts showing the smallest changes in these antioxidants, with the authors suggesting increased symbiont production and translocation (Chan et al. 2025).

Cytochrome c is a key mitochondrial protein facilitating electron transport between complex III (cytc reductase) and complex IV (cytochrome oxidase), integral to the electron transport chain, oxidative phosphorylation, and ATP production (Dunn et al. 2012). Electron leakage can generate ROS and cause cellular damage through peroxidation. Cytochrome c plays an important role in the removal of potentially damaging free radicals that are generated in the mitochondria by accepting electrons from superoxide radicals and delivering them to complex IV (Dunn et al. 2012). Down regulation of these electron transfer proteins could indicate disassembly of electron transfer between complex III and IV. This disassembly of electron transfer has also been observed in *Exaiptasia* under conditions of thermal stress, coupled with enhanced production of cellular ROS (Dunn et al. 2012).

The increase in GSH metabolism observed in SS8 hosts in the current study, which was coupled with the decline in expression of oxidative phosphorylation, is consistent with potential thermal stress front-loading relative to both WT10 and SS5 hosts and potentially reflects a less efficient symbiont photosynthesis that generates less oxidative stress, which is compensated through increased usage of glycolytic ATP.

Amino acid biosynthesis and metabolism

In SS8 hosts relative to WT10, we observed widespread differences in analytes associated with nitrogen assimilation, and metabolism and biosynthesis of amino acids and purines. Specifically, downregulation of glutamine synthetase, which is critical to ammonium assimilation into glutamine, characterised SS8 hosts (DIABLO analysis). This was coupled with a decline in pool size of the associated metabolite, glucosamine-6-phosphate, which is in turn generated from glutamine, and via the pentose phosphate pathway, and can be used to generate ammonium, and to metabolites associated with *de novo* serine biosynthesis, the largest to the 3-phosphoglyceric acid, and the pyruvate precursor, phosphoenolpyruvic acid (PEP), coupled to a downregulation of D-3-phosphoglycerate dehydrogenase. Whereas proteins associated with the metabolism of glycine, serine, and threonine and the oxidation of choline were upregulated (betaine-homocysteine S-methyltransferase 1, sarcosine dehydrogenase, phosphoserine aminotransferase, glycine cleavage system H protein), with associated declines in pool size of the amino acid, L-threonine.

The host driven assimilation of waste ammonium using symbiont-derived carbon, serves as a self-regulating mechanism to control symbiont density through nitrogen availability (Xiang et al. 2020; Cui et al. 2023; Rädecker et al. 2023). Symbiotic anemones utilise glucose and waste ammonium to synthesise serine and glycine via 3-phosphoglycerate and downregulate genes catalysing glycine/serine biosynthesis from food-derived choline via betaine (Cui et al. 2018). Symbiosis also results in upregulation of phosphoserine aminotransferase, which provides amino groups for the biosynthesis of amino acids via the conversion from glutamate to 2-oxoglutarate, in turn inducing ammonium assimilation through glutamine synthetase/glutamate synthase cycle (Cui et al. 2018). In contrast, *Exaiptasia* hosts of *D. trenchii* exhibited minimal expression of glutamine synthetases but had higher expression of methionine-synthesizing betaine–homocysteine S-methyltransferases compared to hosts

of the homologous symbiont *B. minutum* (Sproles et al. 2019). Our results therefore suggest host driven ammonium assimilation via glutamine synthetase to be downregulated with SS8 and indicate a lower availability of waste ammonium and glucose for the biosynthesis of amino acids, with upregulation of alternative pathways for amino acid biosynthesis, of serine, glycine and methionine.

Further, we observed characteristic declines in the relative abundance of the purine metabolite, guanosine, in SS8 hosts relative to WT10 (DIABLO analysis), this was coupled to increased expression of the purine catabolism and salvage proteins (purine nucleoside phosphorylase, adenylate kinase-like). Our concurrent study (Tsang Min Ching et al. 2022) revealed differences in nitrogen storage abilities between the homologous strain and *Cladocopium*, with the relative abundances of purine metabolites and uric acid elevated in *Cladocopium*. It was proposed that these nitrogen stores would enable the maintenance of photosynthesis for symbiont growth under conditions of nitrogen limitation. These enhanced nitrogen storage abilities via purine metabolism could therefore serve to circumvent mechanisms of host control via nitrogen limitation, enabling SS8 persistence.

Transmembrane transport and lysosomal activity

We observed consistent differences to proteins associated with nutrient transport, primarily a downregulation of transmembrane proteins, lysosomal acid hydrolases (proteases and sulfatases), those associated with the transport of lysosomal enzymes, and endocytosis. The largest change was to the active membrane transporter, major facilitator superfamily (MFS) profile domain-containing protein (an organic cation transporter-like protein). However, declines were also observed to phospholipid-transporting ATPase, NPC intracellular cholesterol transporter 2 (NPC2), ABC transporter, in addition to V-type proton ATPase, tetraspanin-33, and sensory neuron membrane protein 2.

In the symbiosis, transmembrane proteins are critical to the exchange of organic and inorganic nutrients between symbiotic partners, and to symbiont photosynthesis; they may also act in symbiont recognition and persistence (Davy et al. 2012). In addition, dinoflagellate cells are encapsulated in a membrane complex of algal and host origin, within the host cnidarian's gastrodermis, termed the symbiosome (Wakefield et al. 2000). Symbiosomes functionally resemble lysosomes as core nutrient sensing and signalling hubs where symbiont-provided nutrients are detected to adapt host physiology (Voss et al. 2019; Voss et al. 2023). MFS include glucose transporters (GLUT) proteins, which have been suggested as the primary mechanism for glucose uptake in *Exaiptasia*, organic cation transporters form a clade of solute transporters within this major group and are located exclusively on the symbiosome membrane (Sproles et al. 2018).

NPC2 functions in the transfer of symbiont produced sterols and are upregulated in symbiosis, versus aposymbiotic cnidarian partnerships. These proteins are symbiosis specific, accumulate in the symbiosome over time, and indicate a mature symbiosome (Hambleton et al. 2019). Two homologues of NPC2 were detected exclusively in anemones colonised by *B. minutum*, they were undetectable in aposymbiotic anemones, or those colonized with the thermal tolerant but nutritionally sub-optimal symbiont, *Durusdinium trenchii* (ITS2 type D1a) (Sproles et al. 2019). Similarly, V-type proton ATPase

which functions in the host's carbon-concentrating mechanism, are only detected in symbiosis, and is partner specific (Mashini et al. 2022).

As discussed above, both SS5 and SS8 *in hospite* had lower rates of carbon fixation relative to WT10 in coral larvae (Buerger et al. 2020). However, targeted analysis of central carbon metabolites in multiple heat-evolved *E. diaphana* partnerships in our concurrent study (Tsang Min Ching et al. 2022), indicated few differences in host partners relative to WT10. As such, no trade-off in symbiont mobile product provision was observed in *E. diaphana* relative to WT10 (Tsang Min Ching et al. 2022). However, the widespread downregulation of associated proteins for active transport of these products observed in the current study does suggest differences in mobile product exchange in *E. diaphana* under ambient conditions. In contrast, the only membrane-associated protein that showed increased expression with SS8 hosts relative to WT10, alpha-glucosidase, has previously been linked to the digestion of the symbiont cell wall, decreasing with increasing symbiont density during established symbiosis (Yuyama et al. 2018). Omics sampling was conducted at 9 weeks post inoculation, at which point symbiont cell densities differed according to strain type, with high variability amongst individuals. Whereas V-type proton ATPase which functions in the host's carbon-concentrating mechanism, was upregulated relative to SS5, indicating differences between the two heat evolved types.

Signalling and heterotrophy

One of the largest reductions in protein levels observed with the SS8 partnership, relative to the WT10, was a protein that catalyses the formation of the signalling molecule cyclic adenosine monophosphate (cAMP) in response to G-protein signalling, adenylate cyclase. This was also coupled to a large reduction in the purine ribonucleoside monophosphate, adenylsuccinic acid, which is an intermediate in the interconversion of purine nucleotides inosine monophosphate (IMP) and adenosine monophosphate (AMP). We also observed a reduction in expression of a protein central to cGMP biosynthetic process (atrial natriuretic peptide receptor 2), and two proteins associated with the mTOR signalling pathway (RRM domain-containing protein). Notably, the largest pool size decline in analysed metabolites in SS8 hosts was also to the signalling metabolite, 5-methoxytryptamine. Similarly, in SS8 hosts relative to SS5, we observed the largest fold change declines in the metabolites, 5-methoxytryptamine and adenylsuccinic acid, coupled again with a decline with cGMP biosynthesis (atrial natriuretic peptide receptor 2). We also observed small but consistent increases in the expression of adenylate cyclase and those associated with purine metabolism, including purine nucleoside phosphorylase, and adenylate kinase-like. In addition, upregulation of prostaglandin reductase 2, central to lipid signalling arachidonic acid pathways, characterised dissimilarity of SS8 (DIABLO analysis).

G-protein signalling was one of the major differentially enriched processes observed in a combined analysis of transcriptome and metabolome, in *Exaiptasia* colonized with *D. trenchii* (Matthews et al. 2017). It was suggested that this was due to differences in host signal transduction and inter-partner signalling with the heterologous symbiont. However, host adenylate cyclase and cAMP production show a diel cycle, increasing during the day, and in the presence of bicarbonate, and are inhibited by calcium

ions (Barott et al. 2013). As symbiont carbon fixation and production of bicarbonate increases the intracellular pH of the symbiosome and host gastrodermal cells, adenylyl cyclase serves a critical role in regulating acid-base homeostasis and facilitating symbiont photosynthesis (Barott et al. 2013). Further, the ciliary swallowing response during feeding in anemones is also regulated by expression of adenylate cyclase. The protein is activated by reduced glutathione (metabolism of which was increased as discussed above), in turn mediating cAMP control of Ca^{2+} distribution, and increasing binding (Gentleman and Mansour 1974). In addition, the cGMP signalling pathway is also involved in the modulation of feeding (Colasanti and Venturini 1998) and the mTOR pathway in host nutrient sensing and growth (Voss et al. 2023). Thus, the downregulation of cAMP and cGMP production as observed in the SS8 partnership, would serve both to regulate photosymbiont photosynthesis, and to increase cilia beating and heterotrophic feeding. Change between partnerships in the highly conserved signal, 5-methoxytryptamine were also notable. This metabolite also induces muscular contraction in anemones, resembling the respiratory rhythm of coelenteric flushing (Tsang et al. 1997). Lower pool sizes of this important metabolite may indicate increased turnover of this signalling pathway in SS8 hosts, and to a lesser extent SS5. In addition, prostaglandin reductase 2 which was upregulated in SS8 partnerships is central to the metabolism of arachidonic acid, which also participates with GSH to increase heterotrophic feeding in the hydroid, *Hydra vulgaris* (Pierobon et al. 1997).

We also observed differences to SS8 host proteins associated with phosphatidylinositol (PI) signalling. Specifically, increases in inositol monophosphatase 1, which catalyses the hydrolysis of myo-inositol monophosphates to myo-inositol, and intracellular calcium sensor protein, calmodulin isoform X1, coupled with a decline to phosphatidylinositol 4-kinase alpha and to the secondary messengers, inositol polyphosphates (IPP) (multiple inositol polyphosphate phosphatase 1). The PI signalling system is thought to play a key role in the symbiosis and is activated via phosphorylation and dephosphorylation by PI kinases and phosphatases (Ashley et al. 2023). The pathway has a wide variety of roles, regulating key cellular processes by triggering cellular signalling cascades, including those involved in immunity, apoptosis, vesicular trafficking, transmembrane signalling, ion channel regulation, lipid homoeostasis, and organelle identification (Ashley et al. 2023). Widespread differences in these proteins are therefore likely indicative of differences in critical processes in *E. diaphana* function, which were to the greatest extent with the heat-evolved SS8 strain.

Recognition and phagocytosis

We observed changes to multiple proteins associated with symbiont recognition and mechanisms of symbiosis establishment, arrest of phagosomal maturation, and endosomal trafficking. Specifically, in SS8 relative to both SS5 and WT10, increased expression of Rab GDP dissociation inhibitor beta, coupled to declines in Ras-related proteins Rab-23 and Rab-4B. We also observed an increase in expression of the recognition associated protein, calumenin in SS5 hosts.

Rab GDP dissociation inhibitor beta negatively regulates vesicular transport through interaction with Rab GTPase and is necessary for phagocytosis (Dheilly et al. 2011). Calumenin is one of the most

upregulated genes in symbiotic anemones and plays a role in the recognition and tolerance of symbionts (Davy et al. 2012). A homolog of Rab4 (ApRab4) is localized to the symbiosome membrane in symbiotic *Exaiptasia* and associated with both the early endocytic and the perinuclear recycling compartments, and its normal function is required for the organization of the recycling compartments (Hong et al. 2009). The protein is retained on the symbiosome of functional symbionts and is considered as an essential part of the mechanism for the biogenesis of the symbiosome (Hong et al. 2009). Rab4 is also involved in the transfer of essential trace elements, such as iron, whose intracellular mobilization is dependent on vesicle trafficking, and which is responsive to thermal stress (Song et al. 2015). Another homologue of the Ras-related protein Rab2, is a signalling protein that is required for the fusion of late endosomes and lysosomes in *Drosophila*, which was more abundant in anemones colonized by *B. minutum* and *D. trenchii* relative to aposymbiotic anemones (Sproles et al. 2019). To our knowledge little published information exists on the function of Rab-23 in invertebrates. However, Rab23 are known to be involved in cilia formation, transport and signalling in eukaryotes (Lim et al. 2011).

Change in these proteins between partnerships, in particular SS8, indicates a downregulation of symbiont uptake via phagocytosis, coupled to a decline in mature symbiosome formation and the associated transfer of trace elements. Further understanding of these processes is critical in order to facilitate and manipulate rapid host colonisation with heat-evolved strains.

Limitations and application steps

In this study a discovery-based multi-omics approach was applied to investigate differences in *E. diaphana* hosts associated with heterologous symbiont introductions (*C. proliferum)*, two that were heat-evolved (SS5 and SS8), versus a wildtype (WT10). Sampling was limited to a single time point, at which we observed high variability and differences in symbiont densities between algal strains. However after 77 weeks, the heterologous heat evolved strains achieved similar cell densities to the homologous type in *E. diaphana* (Tsang Min Ching et al. 2022).

The study used the anemone model, *E. diaphana*. Though a widely used model for reef building corals, additional work in a range of coral hosts is necessary to further initial model insights. The use of cnidarian hosts that support homologous populations of *C. proliferum* symbionts would be beneficial and enable more comprehensive insight into likely benefits of hosting the heat-evolved, selected strains applied in this study. Further, the small size of anemone individuals applied in this study necessitated pooling of samples, limiting replication, and identification of lower abundance analytes.

The untargeted approach, whilst useful for generating hypotheses, is hindered by availability of reference databases, in particular of lipids. Despite high match factors (> 80%), misidentifications with structurally similar analytes also limit biological interpretation. Owing to the highly sensitive MS platforms applied, a degree of contamination of host, symbiont fractions and the wider microbial holobiont is also evident, though we went to great lengths to purify host and symbiont fractions whilst minimizing the loss of critical biomass. Furthermore, without the application of stable isotope tracers, it is not possible to

confirm if differences in the relative abundance of metabolites relate to increased or decreased flux through a pathway.

Implications

This study generates valuable insights into possible targets for improved performance under future ocean conditions, for more rapid infection success with novel and heterologous types. A strength of the multi-block analysis was the identification of key variables responsible for dissimilarity between strains, some of which were not reflected in fold change differences to mapped pathways, for instance to prostaglandin reductase 2 (arachidonic acid metabolism) and 3-hydroxyanthranilate 3,4-dioxygenase, kynurenine-oxoglutarate transaminase 3 (tryptophan metabolism), as well as analytes that may reflect wider differences in function of the holobiont, such as microbial associated products.

Intervention actions require detailed understanding of functional symbiosis and change associated with heterologous introductions. However, the coral holobiont is highly diverse, complex, dynamic, and often highly specific (e.g., temporally, and spatially) and therefore a reductionist approach has typically been applied to their study, focusing on either a particular partner, or functional level of analysis, e.g., gene, protein, metabolite. At the same time these approaches miss much of the important variability and interconnectivity, which in turn is critical to better understand holobiont function. Therefore, a systems biology approach to the study of holobiont function and targets for future proofing will be a valuable tool to informing future coral reef conservation intervention actions, such as via bioengineering (synthetic biology) approaches, for improved traits and stress tolerance (Iqbal et al. 2021). Potential bioengineering targets as identified in the current study are summarized below (Fig. 4).

Materials and Methods

Experimental Design

GBR-sourced *E. diaphana* (Genotype AIMS4) were inoculated with *C. proliferum* heat evolved selected strains (SS5, SS8), and wild type (WT10), for this and a concurrent study (Tsang Min Ching et al. 2022). The culture, inoculation, sampling and processing of anemone individuals for metabolite analysis have already been outlined in our targeted metabolomics study (Tsang Min Ching et al. 2022). Briefly at 9 weeks post-inoculation, 4 replicate anemone individuals were sub-sampled from each partnership in order to estimate symbiont cell density mg^{-1} host protein using cytometry. Anemone individuals for omics sampling were snap frozen in liquid nitrogen, weighed and pooled (n = 2 genetically identical individuals per sample) to ensure sufficient biomass for analysis. Symbiont and host were then separated via bead-mill homogenization with the addition of chilled MilliQ water (8°C), with repeated centrifugation and wash cycles to purify each fraction (host and symbiont). Each fraction was then freeze dried and then weighed for sample specific normalization. Metabolite extractions from the host fraction were then undertaken via a two-step extraction, first with 80% and the second with 50% MeOH, plus internal standard, L-phenylalanine ^{13}C and L-succinic acid ^{13}C (Sigma-Aldrich) at 0.5 µg mL^{-1}. Host

pooled biological samples (PBQC) were produced using 50 µL aliquots of host metabolite extract. Biological blanks were generated via extractions without biological material. The retained protein pellets were subsequently used for proteomics analysis.

Additional sample preparation for multi-omics analysis

Lipid was fractionated from the metabolite extract via filtration with lipid cartridges (Agilent Captiva EMR-Lipid cartridges, 40 mg, 96 well plate). Captured lipid was then eluted from the cartridges via addition of 1 mL 1:2 DCM:MeOH (v/v) and retained for lipid analysis. For lipid identification, host PBQC were produced using 50 µL aliquots of each host sample. To concentrate the samples prior to analysis, the extracts were dried under a continuous stream of nitrogen gas. Samples were then stored at -80°C until analysis.

Discovery metabolomics workflow

Prior to LC-MS analysis metabolite samples were reconstituted in 50 µL 20% MeOH:MQ (v/v). Metabolite samples were then analysed via an Agilent 6546 Liquid Chromatography Time-of-Flight Mass Spectrometer (LC-QToF) with an Agilent Jet Stream source coupled to an Agilent Infinity II UHPLC system (Agilent Technologies, Santa Clara, CA, USA). Chromatographic separation was achieved by injection (4 µL) of sample onto an Agilent InfinityLab Poroshell 120 HILIC-Z Peek lined column (2.1 × 150 mm, 2.7 µm). Each sample was analysed in positive and negative ionization mode. The method was as Agilent App Note 5994-1492EN, Discovery Metabolomics LC/MS Methods Optimized for Polar Metabolites.

Host PBQC data were used to generate MassHunter Personal Compound Databases (PCDL) for further interrogation of acquired samples using accurate mass and retention time. Collected data were processed using MassHunter Profinder software (Version 8.0, Agilent Technologies, Santa Clara, CA, USA), and putatively identified under the Metabolomics Standards Initiative, level 2 (Sumner et al. 2007), against the Agilent METLIN (MS/MS) Metabolite PCDL (G6825-90008, Agilent Technologies, Santa Clara, CA, USA) and library threshold score of 0.8.

Discovery lipidomics workflow

Prior to LC-MS analysis samples were reconstituted in 50 µL 1:1 MeOH:2-butanol (v/v). Lipids were analysed using an Agilent 6546 Liquid Chromatography Time-of-Flight Mass Spectrometer (LC-QToF) with an Agilent Jet Stream source coupled to an Agilent Infinity II UHPLC system (Agilent Technologies, Santa Clara, CA, USA). Chromatographic separation was achieved by injection (1 µL) of the sample onto an Agilent InfinityLab Poroshell HPH-C18 column (2.0 × 150 mm, 2.7 µm). Each sample was analysed in positive and negative ionization mode. The method was as Agilent App Note 5994-0775EN, Lipidomic Analysis of Human Plasma Using Bond Elut Lipid Extraction with the Agilent 6545 LC/Q-TOF.

PBQC samples were run on Auto MS/MS at collisions of 20 eV and 35 eV. Collected data were processed using MassHunter Profinder software (Version 8.0, Agilent Technologies, USA), and putatively identified

against the Agilent METLIN Lipids PCDL (G6825-90008, Agilent Technologies, Santa Clara, CA, USA) and a curated in-house PCDL based on MS/MS spectra and library threshold score of 0.8.

Discovery proteomics workflow

Total protein was extracted from host cell pellets in 8 M Urea, with 20mM ammonium bicarbonate using a homogenizer (TissueLyser II, Qiagen). Sample specific protein concentration was determined using the Braford Assay kit according to the manufacturer instructions (Bio-Rad) (Bradford 1976). Ten µL (5 µg) of protein was reduced with 1 µL of 15% (w/v) DTT for 30 min at room temperature, then alkylated with 1 µL of 40% (w/v) acrylamide for 30 min at room temperature. Proteins were digested by adding 47 µL of trypsin solution (0.1 µg of trypsin in 25 mM ammonium bicarbonate) and incubated at 37 ˚C for 12 h. The digestion was stopped with addition of 1 µL of 10% (v/v) formic acid and the extract filtered through a 0.22µm filter (Millex-LG, syringe driven filter unit, Merck Millipore). Two hundred ng of the tryptic digested peptides was injected for LC-MS analysis.

The trypsin digested samples were analysed using previous methods (François et al. 2021; François et al. 2022; Ahmed et al. 2025). Briefly, for LC-MS analysis, tryptic peptides were desalted and concentrated with a trap column (PepMap100 C18 5 mm x 300 µm, 5 µm, Thermo Scientific) and separated on a nano column (PepMap100 C18 150 mm x 75 µm, 2 µm, Thermo Scientific) using an UltimateTM 3000 RSLC nano LC system (Thermo Scientific). Mobile phase A consisted of MQ water, and 0.1% (v/v) formic acid and mobile phase B consisted of 80% (v/v) acetonitrile, 19.92% MQ water and 0.08% (v/v) formic acid. Tryptic peptides were eluted using a gradient of 5% to 40% solvent B for 60 minutes and 40% to 99% solvent B for 10 minutes. The eluted peptides were ionized with a Nanospray Flex Ion Source (Thermo Scientific). The spray voltage was set to 2.3 kV and the temperature of the heated capillary was set at 300°C. After ionization, mass spectra (MS1) and tandem mass spectra (MS/MS) analysis was performed using an Orbitrap Fusion MS (Thermo Scientific). MS survey scans of peptide precursors were performed in the Orbitrap detector, and the scan range was 400 to 1500 m/z at resolution of 120 K (at 200 m/z). The target value of automatic gain control (AGC) was set as 4×10^5. The maximum injection time for the MS was 50 ms. MS/MS was performed on the most abundant precursors of charge states 2 + to 7 + with intensity greater than 1×10^5, isolated by the quadrupole with a window of 1.6 m/z. Fragmentation was achieved by high-energy collisional dissociation (HCD), with collision energy of 28%. Fragments were detected in the ion trap detector in rapid scan rate mode. The AGC target was 4×10^3, maximum injection time was 300 ms and the dynamic exclusion was 15 seconds. The instrument was set to run in top speed mode, with a three second cycle for both the MS and MS/MS scans.

Protein Discoverer 2.2 (Thermo Scientific) and Sequest HT search engine were used to identify peptides/proteins and quantify relative abundance of proteins. The spectrum data was searched against the *Aiptasia* (GCF_001417965.1_aiptasia_genome_1.1_protein). Precursor mass tolerance was set to 10 ppm and product ions were searched at 0.6 Da. Three missed tryptic cleavages were allowed. Modification included oxidation (+ 15.995Da), deamidation (+ 0.984 Da), amidation (− 0.984Da), and propionamidation (+ 71.037 Da). Peptide spectral matches were validated using the Percolar algorithm,

based on q-values and 1% false discovery rate (FDR). Relative abundance is calculated from precursor abundance intensity and is normalized from total peptide amount.

Statistical Analysis

Anemone wet weights and symbiont density data at week 9 were compared with a non-parametric Kruskal Wallis test in GraphPad Prism (v10.3.0).

The individual omics data were processed and analysed using multivariate statistics. The untargeted omics data of the current study and the targeted metabolite data from our concurrent study (Tsang Min Ching et al. 2022) were combined, with the targeted metabolite data retained in the instance of any duplicate identifications. The metabolite and lipid data were first normalized to sample dry weight biomass and proteins to total peptide amount. All data sets were then zero treated (1/5 of the minimum positive value of each variable) and filtered (IQR) to remove variables that are unlikely to be of use when modelling the data, using MetaboAnalyst v5.0.

In order to map changes in individual proteins and metabolites to overall pathways (lipid maps are not currently integrated with KEGG), fold changes were generated between WT10 hosts versus the selected strain hosts (SS5 and SS8) in MetaboAnalyst v5.0. These fold changes were then visualized in KEGG pathways via Omics Visualization v2.2. Significant protein fold change data were further interrogated via use of gene ontology (GO) terms, associated cellular components, molecular function and biological process where then matched to UniProt identifications via the database conversion bioDBnet (db2db) (Mudunuri et al. 2009). Gene enrichment of upregulated and downregulation proteins were then conducted with KEGG BlastKOALA (Kanehisa et al. 2016).

To examine data structures (lipidomics, proteomics and metabolomics), we performed an unsupervised principal component analysis (PCA) on the normalized data (see above) of the *E. diaphana* hosts in symbiosis with the different symbiont strains (SS5, SS8, WT10) using the mixOmics R package, version 6.28.0 (Rohart et al. 2017). The three omics data sets were then integrated into a metanalysis using a DIABLO (Data Integration Analysis for Biomarker discovery using Latent components) (Singh et al. 2019). The aim of this supervised multiblock sparse PLS-DA was to identify data signatures that are representative of *E. diaphana* hosts in symbiosis with the respective strains and further investigate the relationships between the omic layers. The DIABLO model was set up with a correlation of 0.1 to find the most predictive signatures between the data sets. Model performance was assessed using 5-fold cross validation with 100 repeats using the perf function, and the final model was run with 2 components and max.dist metric.

For presentation of the relative abundance (pre-processed individual omic data) of individual analytes of interest, data were tested for normality, where variables failed to meet assumptions of normality after transformation, non-parametric Kruskal-Wallis was used to compare between strains, with correction for multiple tests (Dunns). Where assumptions were met, ANOVA was applied, with correction for multiple tests (Holm Sidak).

Declarations

Acknowledgements

Anemones used in this study were provided by the van Oppen lab at the University of Melbourne. The authors wish to thank Owain Edwards, Wing Chan, and Madeleine van Oppen for their comments on the initial manuscript.

Fig 5 Created in BioRender. Hillyer, K. (2026) https://BioRender.com/atg3dqo

Author contributions:

Conceptualization: KEH, PB

Methodology: KEH, PB, SJTMC, JWL, DJB

Investigation: KEH, PB, SJTMC, JWL

Visualization: KEH, PB, DJB

Supervision: DJB

Writing—original draft: KEH, PB, JWL

Writing—review & editing: KEH, PB, DJB

Competing interests:

The author(s) declare no competing interests.

Data and materials availability:

Data supporting the results is available in the supplementary information.

References

1. Ahmed KA, Yeap HL, Coppin CW, Liu J-W, Pandey G, Taylor PW, Lee SF, Oakeshott JG (2025) Seminal fluid proteins in the Queensland fruit fly: Tissue origins, effects of mating and comparative genomics. Insect Biochemistry and Molecular Biology 177:104247
2. Anthony K, Bay LK, Costanza R, Firn J, Gunn J, Harrison P, Heyward A, Lundgren P, Mead D, Moore T, Mumby PJ, van Oppen MJH, Robertson J, Runge MC, Suggett DJ, Schaffelke B, Wachenfeld D, Walshe T (2017) New interventions are needed to save coral reefs. Nature Ecology & Evolution 1:1420–1422
3. Ashley IA, Kitchen SA, Gorman LM, Grossman AR, Oakley CA, Suggett DJ, Weis VM, Rosset SL, Davy SK (2023) Genomic conservation and putative downstream functionality of the phosphatidylinositol

signalling pathway in the cnidarian-dinoflagellate symbiosis. Frontiers in Microbiology 13:1094255

4. Barott K, Helman Y, Haramaty L, Barron ME, Hess K, Buck J, Levin L, Tresguerres M (2013) High adenylyl cyclase activity and in vivo cAMP fluctuations in corals suggest central physiological role. Sci Rep 3:1379
5. Bradford MM (1976) A rapid and sensitive method for the quantitation of microgram quantities of protein utilizing the principle of protein-dye binding. Analytical Biochemistry 72:248–254
6. Buerger P, Alvarez-Roa C, Coppin CW, Pearce SL, Chakravarti LJ, Oakeshott JG, Edwards OR, van Oppen MJH (2020) Heat-evolved microalgal symbionts increase coral bleaching tolerance. Science Advances 6:eaba2498
7. Burriesci MS, Raab TK, Pringle JR (2012) Evidence that glucose is the major transferred metabolite in dinoflagellate–cnidarian symbiosis. Journal of Experimental Biology 215:3467–3477
8. Butler CC, Turnham KE, Lewis AM, Nitschke MR, Warner ME, Kemp DW, Hoegh-Guldberg O, Fitt WK, van Oppen MJH, LaJeunesse TC (2023) Formal recognition of host-generalist species of dinoflagellate (Cladocopium, Symbiodiniaceae) mutualistic with Indo-Pacific reef corals. Journal of Phycology 59:698–711
9. Chakravarti LJ, Beltran VH, van Oppen MJH (2017) Rapid thermal adaptation in photosymbionts of reef-building corals. Global Change Biology 23:4675–4688
10. Chan WY, Meyers L, Rudd D, Topa SH, van Oppen MJH (2023) Heat-evolved algal symbionts enhance bleaching tolerance of adult corals without trade-off against growth. Global Change Biology 29:6945–6968
11. Chan WY, Sakamoto R, Doering T, Narayana VK, De Souza DP, McConville MJ, van Oppen MJ (2025) Heat-Evolved Microalgae (Symbiodiniaceae) Are Stable Symbionts and Influence Thermal Tolerance of the Sea Anemone Exaiptasia diaphana. Environmental Microbiology 27:e70011
12. Cleves PA (2022) A Need for Reverse Genetics to Study Coral Biology and Inform Conservation Efforts. In: van Oppen MJH, Aranda Lastra M (eds) Coral Reef Conservation and Restoration in the Omics Age. Springer International Publishing, Cham, pp167–178
13. Colasanti M, Venturini G (1998) Nitric oxide in invertebrates. Molecular neurobiology 17:157–174
14. Cui G, Liew YJ, Li Y, Kharbatia N, Zahran NI, Emwas A-H, Eguiluz VM, Aranda M (2018) Meta-analysis reveals host-dependent nitrogen recycling as a mechanism of symbiont control in Aiptasia. bioRxiv:269183
15. Cui G, Liew YJ, Li Y, Kharbatia N, Zahran NI, Emwas A-H, Eguiluz VM, Aranda M (2019) Host-dependent nitrogen recycling as a mechanism of symbiont control in *Aiptasia*. PLOS Genetics 15:e1008189
16. Cui G, Mi J, Moret A, Menzies J, Zhong H, Li A, Hung S-H, Al-Babili S, Aranda M (2023) A carbon-nitrogen negative feedback loop underlies the repeated evolution of cnidarian–Symbiodiniaceae symbioses. Nat Commun 14:6949
17. Cziesielski MJ, Liew YJ, Cui G, Schmidt-Roach S, Campana S, Marondedze C, Aranda M (2018) Multi-omics analysis of thermal stress response in a zooxanthellate cnidarian reveals the importance of

associating with thermotolerant symbionts. Proceedings of the Royal Society B: Biological Sciences 285:20172654

18. Davy SK, Allemand D, Weis VM (2012) Cell biology of cnidarian-dinoflagellate symbiosis. Microbiol Mol Biol Rev 76:229–261
19. Dheilly NM, Haynes PA, Bove U, Nair SV, Raftos DA (2011) Comparative proteomic analysis of a sea urchin (Heliocidaris erythrogramma) antibacterial response revealed the involvement of apextrin and calreticulin. Journal of invertebrate pathology 106:223–229
20. Dunn SR, Pernice M, Green K, Hoegh-Guldberg O, Dove SG (2012) Thermal Stress Promotes Host Mitochondrial Degradation in Symbiotic Cnidarians: Are the Batteries of the Reef Going to Run Out? PLOS ONE 7:e39024
21. Eichmann TO, Lass A (2015) DAG tales: the multiple faces of diacylglycerol—stereochemistry, metabolism, and signaling. Cellular and Molecular Life Sciences 72:3931–3952
22. François M, Karpe A, Liu J-W, Beale D, Hor M, Hecker J, Faunt J, Maddison J, Johns S, Doecke J, Rose S, Leifert WR (2021) Salivaomics as a Potential Tool for Predicting Alzheimer's Disease During the Early Stages of Neurodegeneration. Journal of Alzheimer's Disease 82:1301–1313
23. François M, Karpe AV, Liu J-W, Beale DJ, Hor M, Hecker J, Faunt J, Maddison J, Johns S, Doecke JD, Rose S, Leifert WR (2022) Multi-Omics, an Integrated Approach to Identify Novel Blood Biomarkers of Alzheimer's Disease. Metabolites 12:949
24. Garrett TA, Hwang J, Schmeitzel JL, Schwarz J (2011) Lipidomics of *Aiptasia pallida* and *Symbiodinium*: A model system for investigating the molecular basis of coral symbiosis. Wiley Online Library
25. Garrett TA, Schmeitzel JL, Klein JA, Hwang JJ, Schwarz JA (2013) Comparative lipid profiling of the cnidarian *Aiptasia pallida* and its dinoflagellate symbiont. PloS one 8:e57975
26. Gentleman S, Mansour TE (1974) Adenylate cyclase in sea anemone implication for chemoreception. Biochimica et Biophysica Acta (BBA)-General Subjects 343:469–479
27. Hambleton EA, Jones VAS, Maegele I, Kvaskoff D, Sachsenheimer T, Guse A (2019) Sterol transfer by atypical cholesterol-binding NPC2 proteins in coral-algal symbiosis. Elife 8:e43923
28. Hillyer KE, Tumanov S, Villas-Bôas S, Davy SK (2016) Metabolite profiling of symbiont and host during thermal stress and bleaching in a model cnidarian–dinoflagellate symbiosis. Journal of Experimental Biology 219:516–527
29. Hillyer KE, Dias DA, Lutz A, Roessner U, Davy SK (2017) Mapping carbon fate during bleaching in a model cnidarian symbiosis: the application of ^{13}C metabolomics. New Phytologist 214:1551–1562
30. Hillyer KE, Dias D, Lutz A, Roessner U, Davy SK (2018) ^{13}C metabolomics reveals widespread change in carbon fate during coral bleaching. Metabolomics 14:12
31. Hong M-C, Huang Y-S, Song P-C, Lin W-W, Fang L-S, Chen M-C (2009) Cloning and characterization of ApRab4, a recycling Rab protein of Aiptasia pulchella, and its implication in the symbiosome biogenesis. Marine biotechnology 11:771–785

32. Hughes TP, Kerry JT, Baird AH, Connolly SR, Dietzel A, Eakin CM, Heron SF, Hoey AS, Hoogenboom MO, Liu G, McWilliam MJ, Pears RJ, Pratchett MS, Skirving WJ, Stella JS, Torda G (2018) Global warming transforms coral reef assemblages. Nature 556:492–496
33. Hughes TP, Kerry JT, Baird AH, Connolly SR, Chase TJ, Dietzel A, Hill T, Hoey AS, Hoogenboom MO, Jacobson M, Kerswell A, Madin JS, Mieog A, Paley AS, Pratchett MS, Torda G, Woods RM (2019) Global warming impairs stock–recruitment dynamics of corals. Nature
34. Iqbal Z, Iqbal MS, Khan MIR, Ansari MI (2021) Toward integrated multi-omics intervention: rice trait improvement and stress management. Frontiers in Plant Science 12
35. Kanehisa M, Sato Y, Morishima K (2016) BlastKOALA and GhostKOALA: KEGG Tools for Functional Characterization of Genome and Metagenome Sequences. Journal of Molecular Biology 428:726–731
36. Liang J, Luo W, Yu K, Xu Y, Chen J, Deng C, Ge R, Su H, Huang W, Wang G (2022) Multi-Omics Revealing the Response Patterns of Symbiotic Microorganisms and Host Metabolism in Scleractinian Coral *Pavona minuta* to Temperature Stresses. Metabolites 12:18
37. Lim YS, Chua CEL, Tang BL (2011) Rabs and other small GTPases in ciliary transport. Biology of the Cell 103:209–221
38. Maruyama T, Ito M, Wakaoji S, Okubo Y, Ide K, Nishikawa Y, Fujimura H, Suda S, Nakano Y, Satoh N, Shinzato C, Yura K, Takeyama H (2021) Multi-omics analysis reveals cross-organism interactions in coral holobiont. bioRxiv:2021.2010.2025.465660
39. Mashini AG, Oakley CA, Grossman AR, Weis VM, Davy SK (2022) Immunolocalization of metabolite transporter proteins in a model cnidarian-dinoflagellate symbiosis. Applied and Environmental Microbiology 88:e00412-00422
40. Matthews JL, Oakley CA, Lutz A, Hillyer KE, Roessner U, Grossman AR, Weis VM, Davy SK (2018) Partner switching and metabolic flux in a model cnidarian dinoflagellate symbiosis. Proceedings of the Royal Society B: Biological Sciences 285:20182336
41. Matthews JL, Crowder CM, Oakley CA, Lutz A, Roessner U, Meyer E, Grossman AR, Weis VM, Davy SK (2017) Optimal nutrient exchange and immune responses operate in partner specificity in the cnidarian-dinoflagellate symbiosis. Proceedings of the National Academy of Sciences 114:13194–13199
42. Mudunuri U, Che A, Yi M, Stephens RM (2009) bioDBnet: the biological database network. Bioinformatics (Oxford, England) 25:555–556
43. Nitschke MR, Abrego D, Allen CE, Alvarez-Roa C, Boulotte NM, Buerger P, Chan WY, Fae Neto WA, Ivory E, Johnston B, Meyers L, Parra V C, Peplow L, Perez T, Scharfenstein HJ, van Oppen MJH (2024) The use of experimentally evolved coral photosymbionts for reef restoration. Trends in Microbiology 32:1241–1252
44. Oakley CA, Ameismeier MF, Peng L, Weis VM, Grossman AR, Davy SK (2016) Symbiosis induces widespread changes in the proteome of the model cnidarian *Aiptasia*. Cellular Microbiology 18:1009–1023

45. Palumbi SR, Barshis DJ, Traylor-Knowles N, Bay RA (2014) Mechanisms of reef coral resistance to future climate change. Science 344:895–898
46. Pierobon P, De Petrocellis L, Minei R, Di Marzo V (1997) Arachidonic acid as an endogenous signal for the glutathione-induced feeding response in Hydra. Cellular and Molecular Life Sciences CMLS 53:61–68
47. Quigley KM, Alvarez-Roa C, Raina J-B, Pernice M, van Oppen MJH (2023) Heat-evolved microalgal symbionts increase thermal bleaching tolerance of coral juveniles without a trade-off against growth. Coral Reefs 42:1227–1232
48. Rädecker N, Escrig S, Spangenberg JE, Voolstra CR, Meibom A (2023) Coupled carbon and nitrogen cycling regulates the cnidarian–algal symbiosis. Nat Commun 14:6948
49. Rohart F, Gautier B, Singh A, Lê Cao K-A (2017) mixOmics: An R package for 'omics feature selection and multiple data integration. PLOS Computational Biology 13:e1005752
50. Rosset SL, Oakley CA, Ferrier-Pagès C, Suggett DJ, Weis VM, Davy SK (2021) The Molecular Language of the Cnidarian–Dinoflagellate Symbiosis. Trends in Microbiology 29:320–333
51. Singh A, Shannon CP, Gautier B, Rohart F, Vacher M, Tebbutt SJ, Lê Cao K-A (2019) DIABLO: an integrative approach for identifying key molecular drivers from multi-omics assays. Bioinformatics 35:3055–3062
52. Song P-C, Wu T-M, Hong M-C, Chen M-C (2015) Elevated temperature inhibits recruitment of transferrin-positive vesicles and induces iron-deficiency genes expression in Aiptasia pulchella host-harbored Symbiodinium. Comparative Biochemistry and Physiology Part B: Biochemistry and Molecular Biology 188:1–7
53. Sproles AE, Kirk NL, Kitchen SA, Oakley CA, Grossman AR, Weis VM, Davy SK (2018) Phylogenetic characterization of transporter proteins in the cnidarian-dinoflagellate symbiosis. Molecular Phylogenetics and Evolution 120:307–320
54. Sproles AE, Oakley CA, Matthews JL, Peng L, Owen JG, Grossman AR, Weis VM, Davy SK (2019) Proteomics quantifies protein expression changes in a model cnidarian colonised by a thermally tolerant but suboptimal symbiont. ISME J 13:2334–2345
55. Sumner LW, Amberg A, Barrett D, Beale MH, Beger R, Daykin CA, Fan TWM, Fiehn O, Goodacre R, Griffin JL, Hankemeier T, Hardy N, Harnly J, Higashi R, Kopka J, Lane AN, Lindon JC, Marriott P, Nicholls AW, Reily MD, Thaden JJ, Viant MR (2007) Proposed minimum reporting standards for chemical analysis Chemical Analysis Working Group (CAWG) Metabolomics Standards Initiative (MSI). Metabolomics 3:211–221
56. Tsang Min Ching SJ, Chan WY, Perez-Gonzalez A, Hillyer KE, Buerger P, van Oppen MJH (2022) Colonization and metabolite profiles of homologous, heterologous and experimentally evolved algal symbionts in the sea anemone *Exaiptasia diaphana*. ISME Communications 2:30
57. Tsang WH, McGaughey N, Wong YH, Wong JT (1997) Melatonin and 5-methoxytryptamine induced muscular contraction in sea anemones. Journal of Experimental Zoology 279:201–207

58. van Oppen MJH, Blackall LL (2019) Coral microbiome dynamics, functions and design in a changing world. Nat Rev Microbiol 17:557–567
59. van Oppen MJH, Oliver JK, Putnam HM, Gates RD (2015) Building coral reef resilience through assisted evolution. Proceedings of the National Academy of Sciences 112:2307–2313
60. Voss PA, Gornik SG, Jacobovitz MR, Rupp S, Dörr MS, Maegele I, Guse A (2019) Nutrient-dependent mTORC1 signaling in coral-algal symbiosis. bioRxiv:723312
61. Voss PA, Gornik SG, Jacobovitz MR, Rupp S, Dörr M, Maegele I, Guse A (2023) Host nutrient sensing is mediated by mTOR signaling in cnidarian-dinoflagellate symbiosis. Current Biology 33:3634–3647. e3635
62. Wakefield TS, Farmer MA, Kempf SC (2000) Revised description of the fine structure of in situ" zooxanthellae" genus Symbiodinium. The Biological Bulletin 199:76–84
63. Weis VM, Davy SK, Hoegh-Guldberg O, Rodriguez-Lanetty M, Pringle JR (2008) Cell biology in model systems as the key to understanding corals. Trends in ecology & evolution 23:369–376
64. Xiang T, Lehnert E, Jinkerson RE, Clowez S, Kim RG, DeNofrio JC, Pringle JR, Grossman AR (2020) Symbiont population control by host-symbiont metabolic interaction in Symbiodiniaceae-cnidarian associations. Nat Commun 11:108
65. Yan Z, Chen B, Yang Y, Yi X, Wei M, Ecklu-Mensah G, Buschmann MM, Liu H, Gao J, Liang W, Liu X, Yang J, Ma W, Liang Z, Wang F, Chen D, Wang L, Shi W, Stampfli MR, Li P, Gong S, Chen X, Shu W, El-Omar EM, Gilbert JA, Blaser MJ, Zhou H, Chen R, Wang Z (2022) Multi-omics analyses of airway host–microbe interactions in chronic obstructive pulmonary disease identify potential therapeutic interventions. Nature Microbiology 7:1361–1375
66. Yuyama I, Ishikawa M, Nozawa M, Yoshida M-a, Ikeo K (2018) Transcriptomic changes with increasing algal symbiont reveal the detailed process underlying establishment of coral-algal symbiosis. Sci Rep 8:16802

Table 2

Table 2 is available in the Supplementary Files section.

Figures

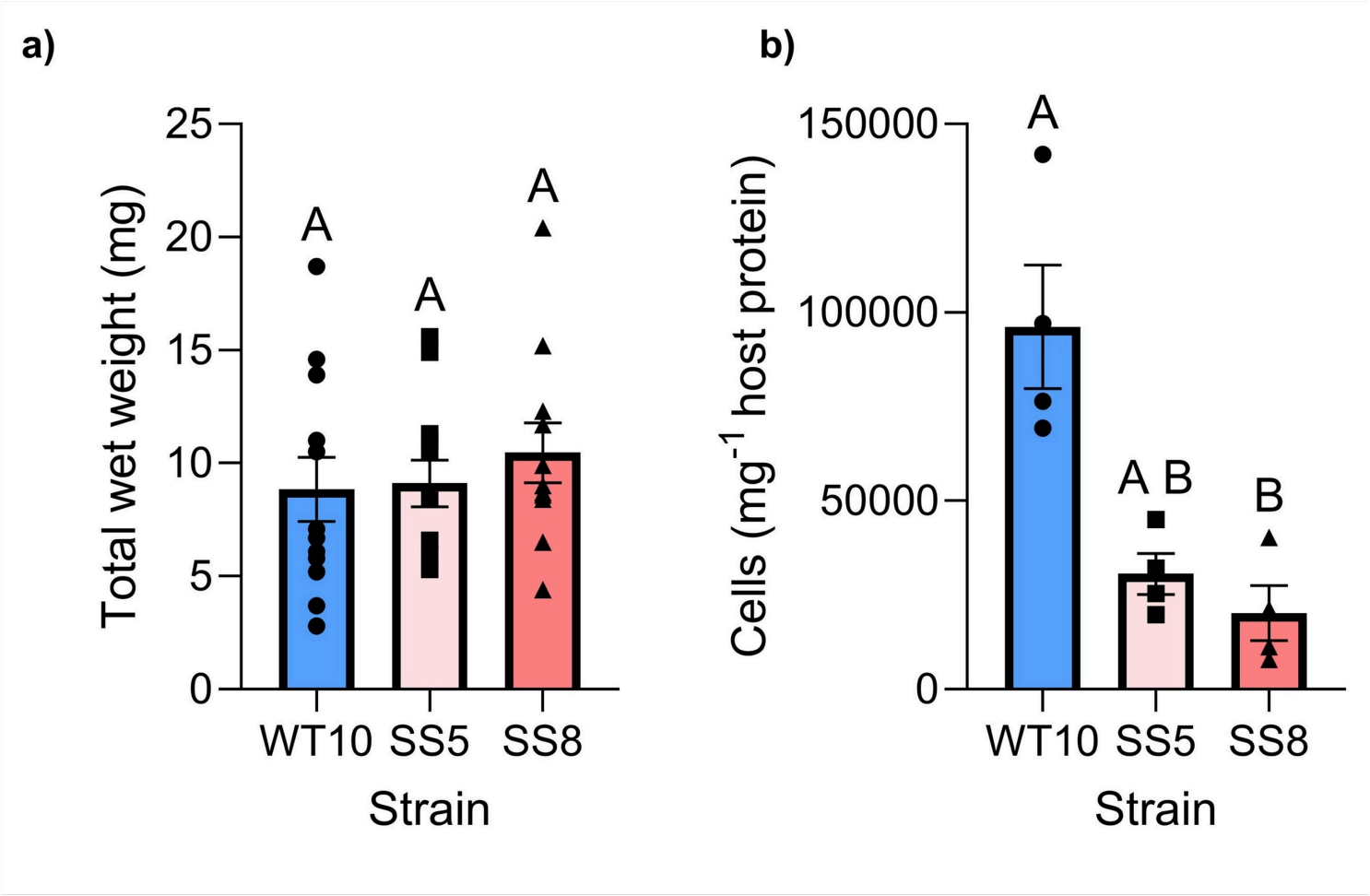

Figure 1

a). Analysed anemone total wet weights (n=35; mg); and b). Symbiont cell density (n=12; cells mg^{-1} host protein) by symbiont strain type. Symbiont Cladocopium proliferum types: wildtype 10 (WT10), heat evolved selected strain 5 (SS5) and selected strain 8 (SS8) (Kruskal Wallis groups)

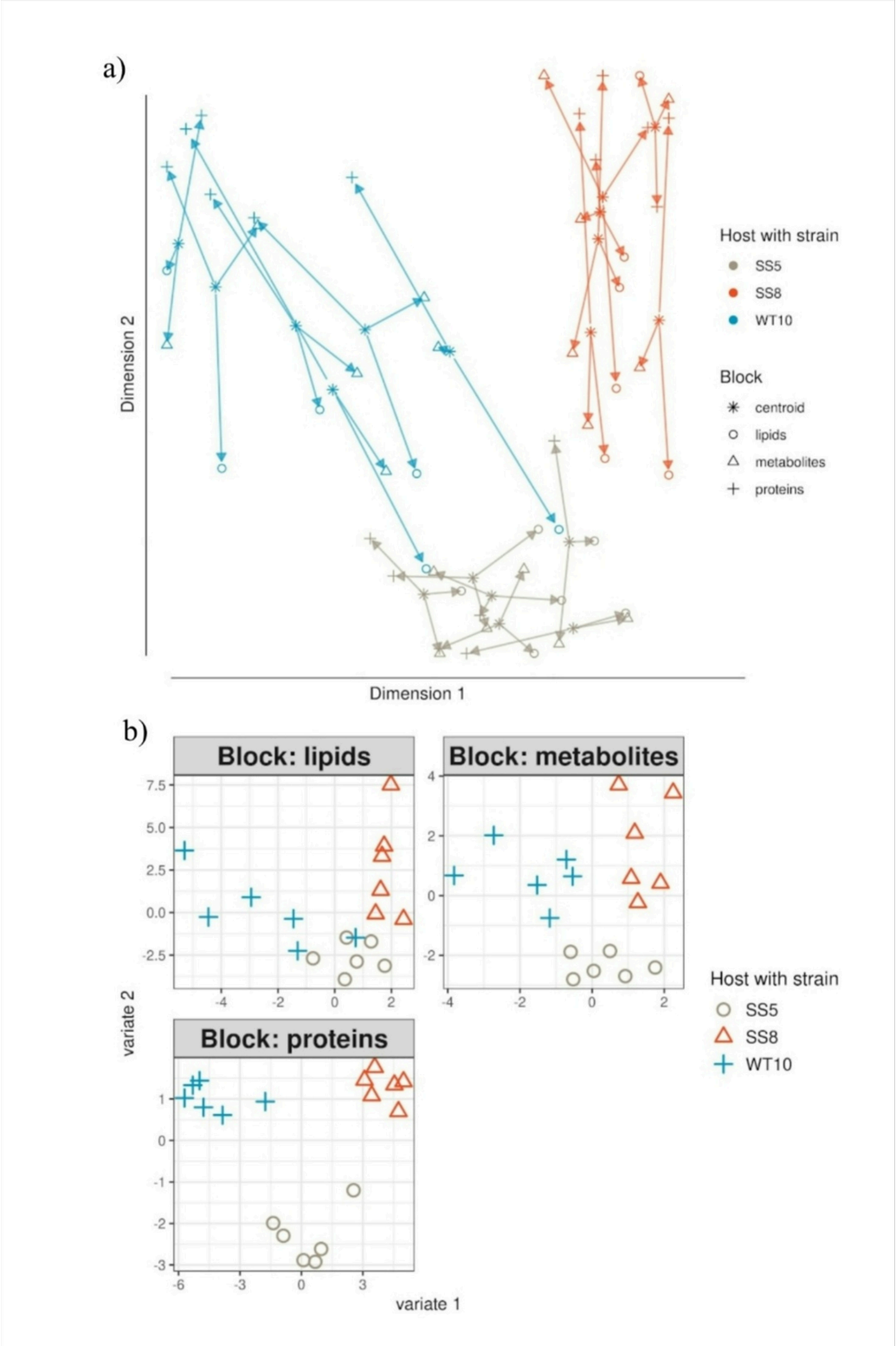

Figure 2

Multi-block PLS-DA (DIABLO) analysis of E. diaphana host protein, lipid and metabolite data, coloured according to symbiont strain (C. proliferum SS5, SS8, and WT10); a) combined plot showing the sample average across the respective data sets as centroids, b) individual plots for the respective data.

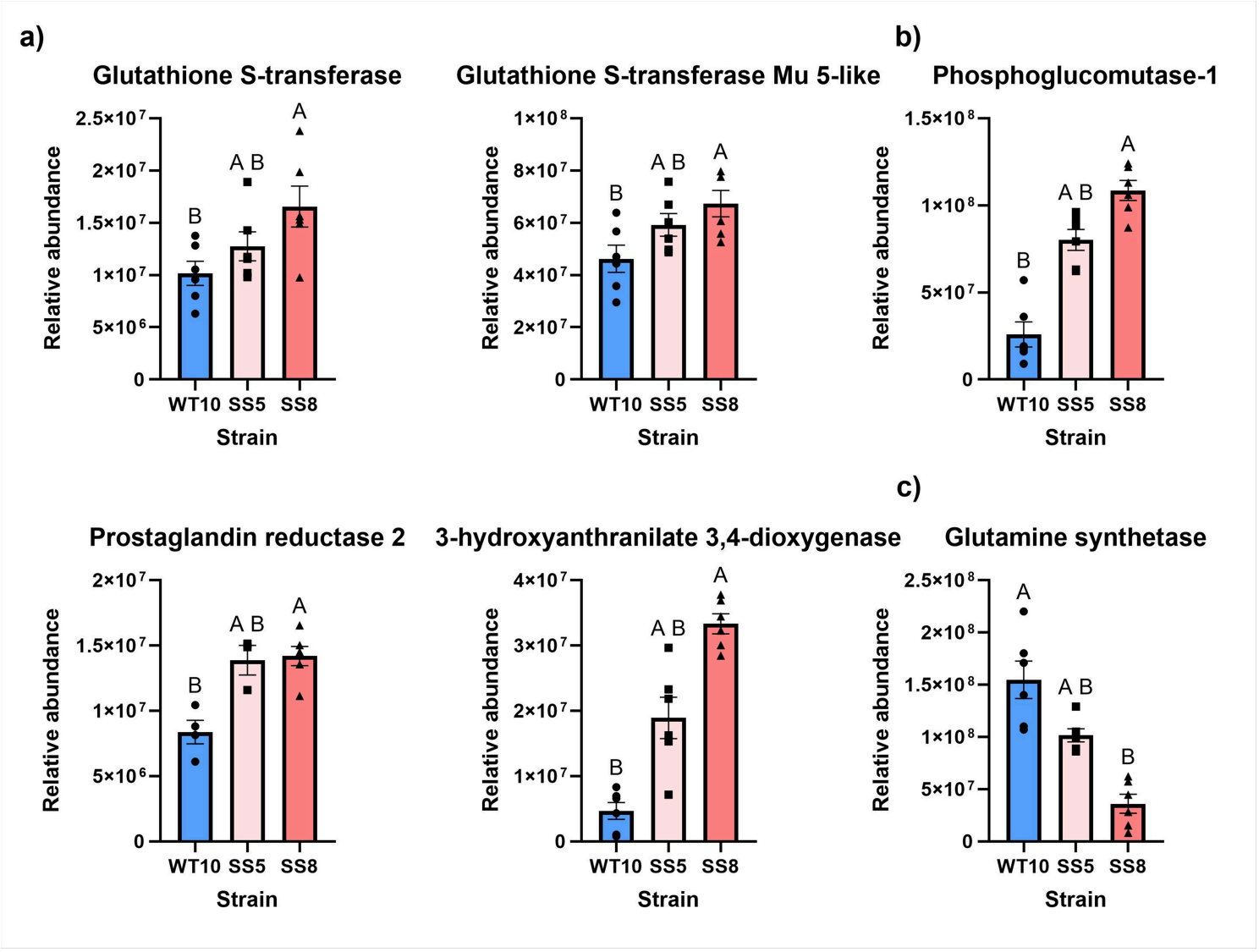

Figure 3

Key differentiated proteins between WT10 and SS8 hosts, as identified by DIABLO analysis (Kruskal-Wallis groups)

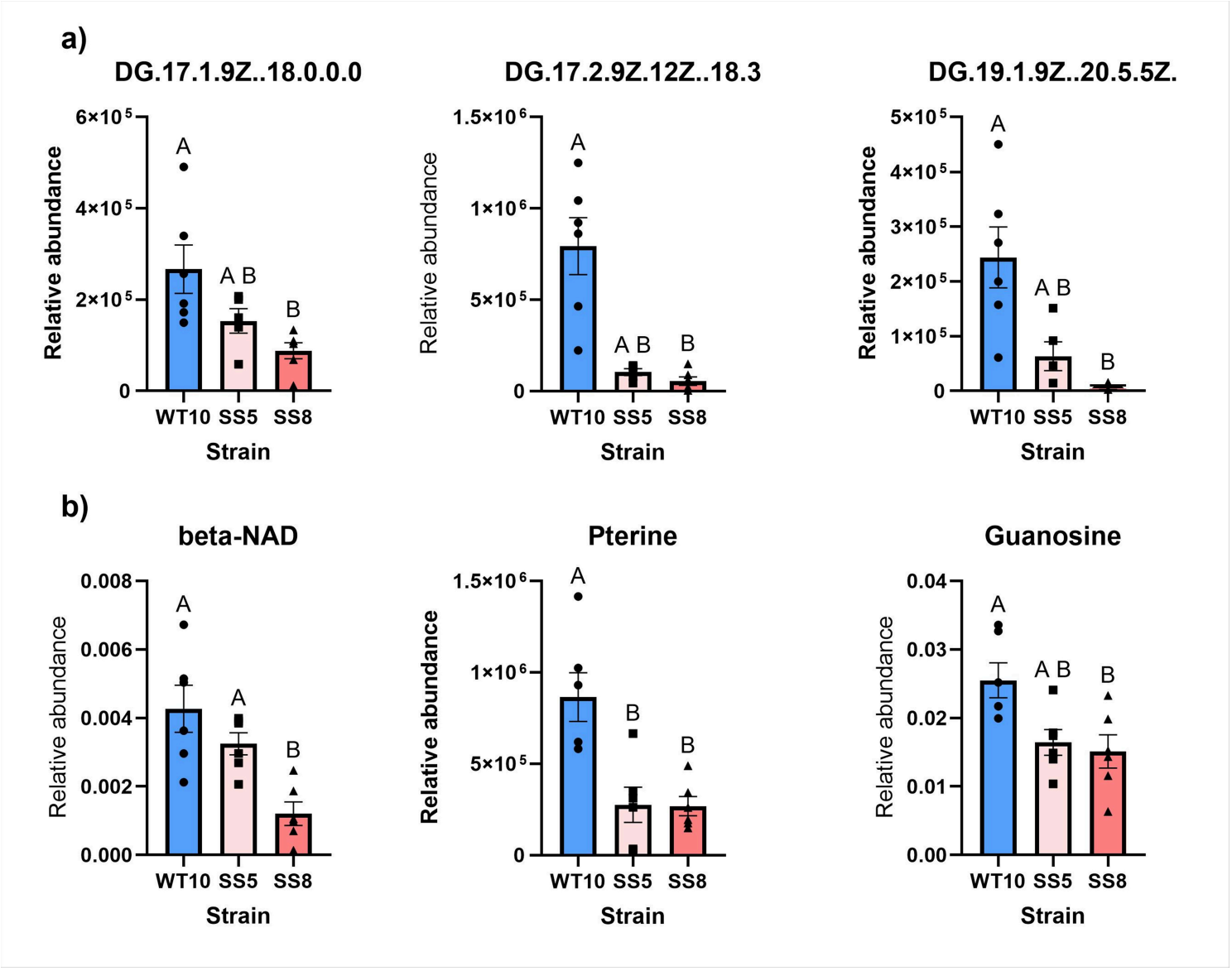

Figure 4

Key differentiated a) lipids and b) metabolites between WT10 and SS8 E. diaphana hosts, as identified by DIABLO analysis (Kruskal-Wallis groups)

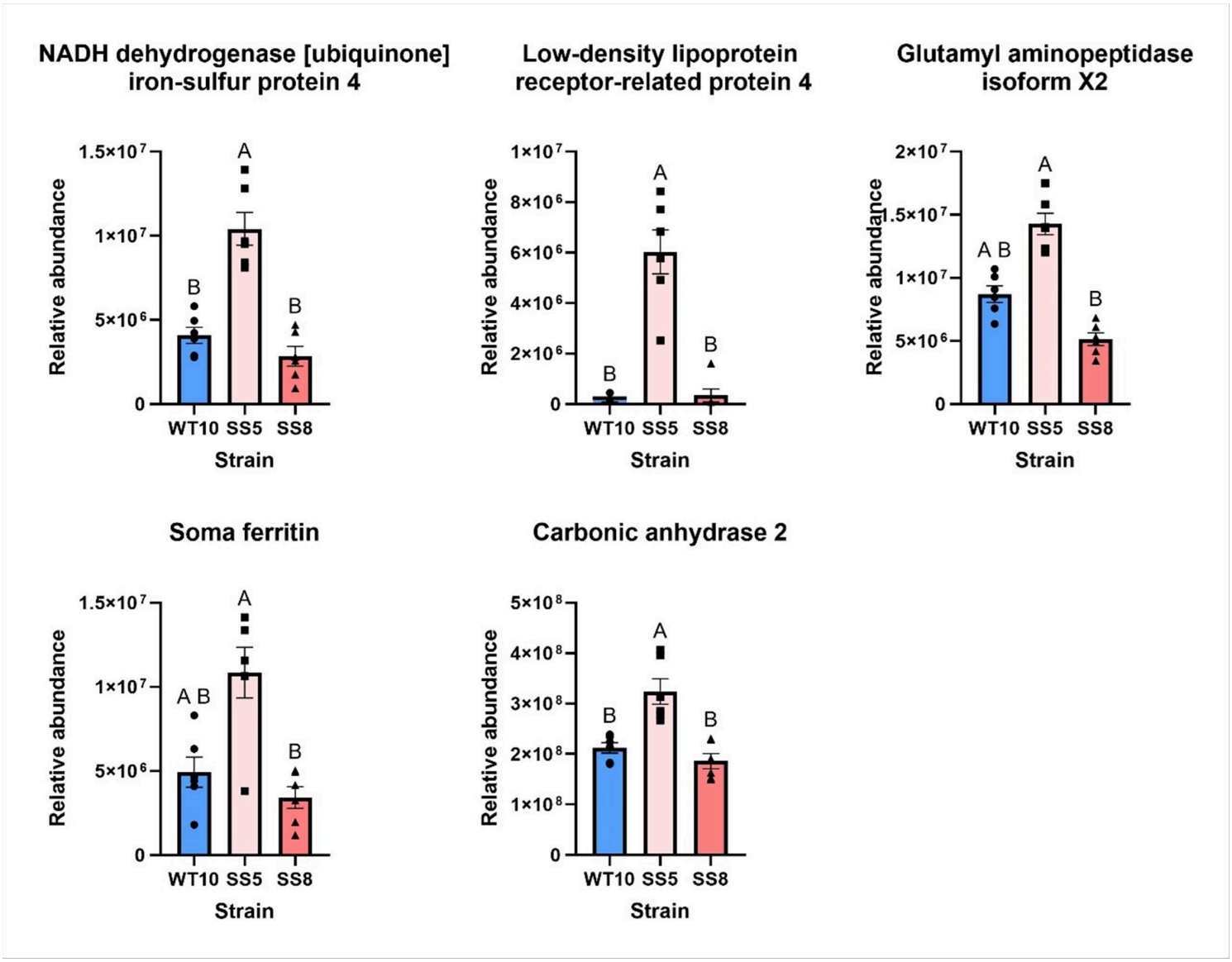

Figure 5

Key differentiated proteins in SS5 E. diaphana hosts, as identified by DIABLO analysis. Differences in relative abundance as identified by letter display (Kruskal-Wallis groups)

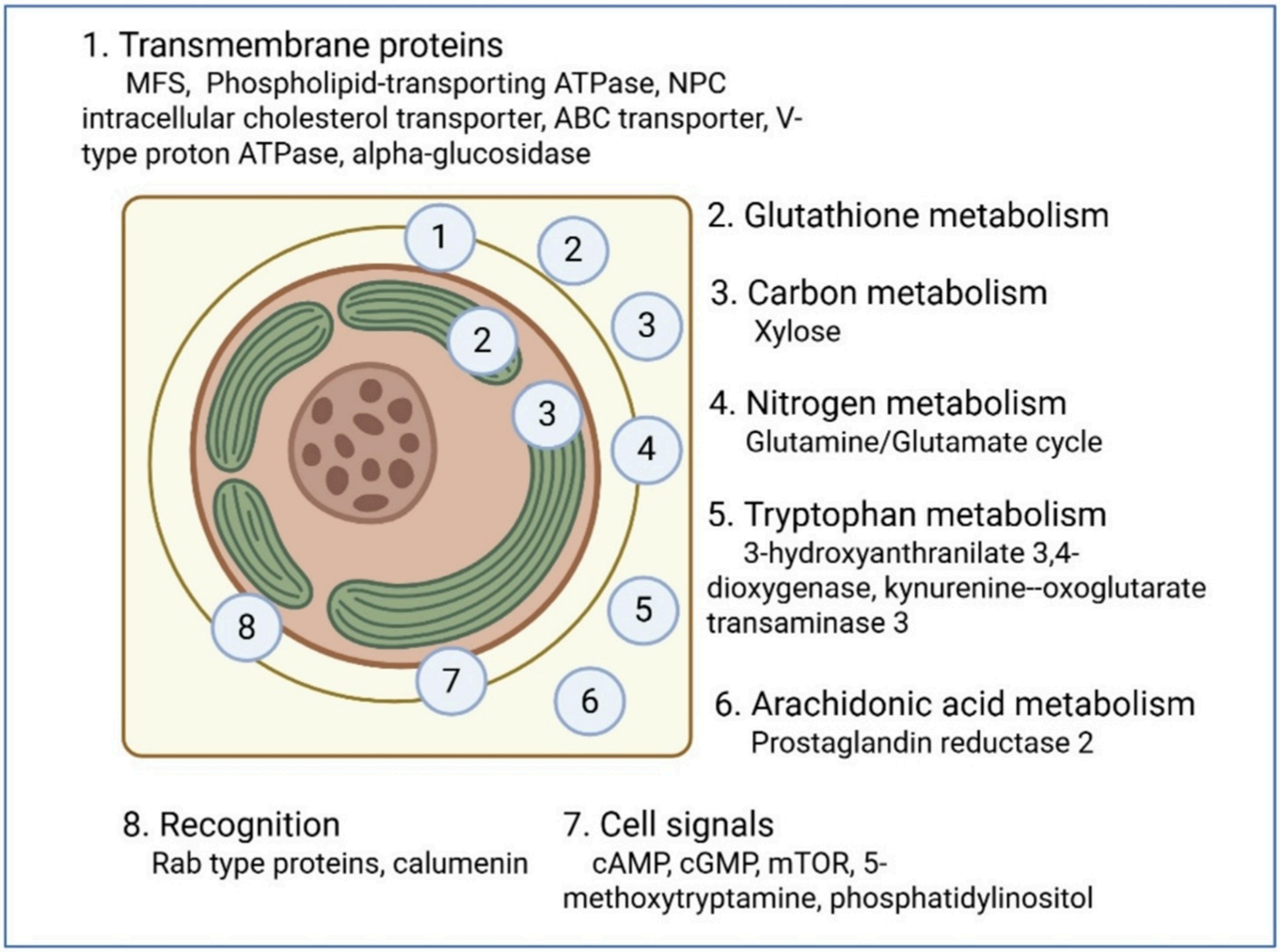

Figure 6

Considerations for synthetic biology interventions generated by multi-omics analysis of wild type and heat-evolved symbiont partners

Supplementary Files

This is a list of supplementary files associated with this preprint. Click to download.

- SI20260421.docx
- Table2.docx